Dynamics of nonergodic ferromagnetic/antiferromagnetic ordering and magnetocaloric in antiperovskite Mn_3SnC

Ö. Çakır,[1] F. Cugini,[2] M. Solzi,[2] K. Priolkar,[3] M. Acet,[4,*] and M. Farle[4,5]

[1]*Physics Department, Yildiz Technical University, 34220 Esenler, Istanbul, Turkey*

[2]*Department of Mathematical, Physical and Computer Sciences, University of Parma, Parco Area delle Scienze 7/A, 43124 Parma, Italy*

[3]*Department of Physics, Goa University Taleigao Plateau, 403206 Goa, India*

[4]*Experimentalphysik, University of Duisburg-Essen, 47048 Duisburg, Germany*

[5]*Center for Functionalized Magnetic Materials, Immanuel Kant Baltic Federal University, Kaliningrad, Russian Federation*

(Received 9 June 2017; published 28 July 2017)

We investigated the time dependence of the magnetic configuration at the mixed magnetic magnetostructural transition in Mn_3SnC. The nonergodic nature of the transition involves the stabilization of a final magnetic configuration that involves additional AF ordering which is not present when the transition is initiated and develops only in time. We show the presence of the nonergodicity over a time scale of about 1 hour by field and time-dependent magnetization studies. Two characteristic times related to the transition are observed. We also study the equilibrium thermodynamics under ergodic conditions by heat capacity studies and determine the entropy-change and the adiabatic temperature change around the transition. We find agreement between the indirect and direct methods in determining the adiabatic temperature change and discuss the influence of nonergodic properties on the magnetocaloric effects.

DOI: 10.1103/PhysRevB.96.014436

I. INTRODUCTION

Antiperovskite intermetallic compounds in the form M_3AX (M: transition metal, A: main group element, X: carbon, boron, or nitrogen;) display many interesting properties, such as superconductivity [1,2], giant magnetoresistance [3], giant negative thermal expansion [4,5], and large inverse magnetocaloric effects [6–8]; all which are important functionalities relevant for applications. In many cases, these properties are closely related to the presence of a first-order magnetostructural phase transition.

In particular, Mn-based antiperovskites exhibit interesting magnetic ordering properties and undergo various magnetic phase transitions. Among them, Mn_3AC (A: Ga, In, Zn) undergo a multitude of complex magnetic transitions [9–14], and recently, it has been shown that the antiperovskite Mn_3SnC stands out somewhat differently with its characteristic magnetic structure [15]. Mn_3SnC undergoes a first-order magnetostructural transition near room temperature from a high-temperature paramagnetic (PM) state to a low-temperature, magnetically complex ordered state accompanied by a narrow thermal hysteresis. The volume of the high-temperature state is smaller than that of the low-temperature state; the states being isostructural. The complexity of the magnetic structure is related to the fact that there are two types of Mn atoms, Mn1 and Mn2, located at the face centers of the antiperovskite cube. The moments of the Mn1 species align ferromagnetically with a moment of 0.7 μ_B along the 001 direction, whereas those of Mn2 align antiferromagnetically with a moment of 2.4 μ_B in the a-b plane perpendicular to 001.

Mn-based antiperovskite compounds also exhibit substantial magnetocaloric effects around their magnetostructural transitions with entropy changes, ΔS, of about 80 mJ cm^3 K^{-1} under a magnetic-field change of 2 T [6,16,17]. Mn_3SnC compounds doped with other main group elements have been investigated for their magnetocaloric effects, and it was found that these materials can be appropriate for magnetic refrigeration [18]. However, in order to control and optimize magnetocaloric effects around first-order magnetostructural transitions, it is necessary to understand the details of the mechanism of the transition and any hysteresis effects associated with it. Here, our aim is to investigate the dynamics of the phase transition leading to the complex magnetic structure of Mn_3SnC and how the complexities relate to magnetocaloric effects. We study the dynamics of the transition by magnetization measurements as a function of temperature $M(T)$, field $M(B)$, and time $M(t)$, and the magnetocaloric properties by temperature and field-dependent heat capacity $c_p(T)$, and temperature-dependent direct adiabatic temperature-change measurements $\Delta T(T)$.

II. EXPERIMENTAL

The Mn_3SnC sample used in the experiments was prepared using manganese, tin, and graphite powders with purity of at least 99.95% as starting materials. They were mixed in the stoichiometric proportion and pressed into a pellet. The pellet was sealed in a quartz tube under argon atmosphere, and it was sintered in a furnace at 800 °C for 5 days. It was then cooled down to room temperature. The grinding, pressing and heat treating procedure was repeated three times. The magnetization as a function of temperature $M(T)$ in the range $5 \leqslant T \leqslant 300$ K and as a function of magnetic field $M(B)$ up to 5 T were carried out using a superconducting quantum interference magnetometer. The ac susceptibility, χ_{ac}, measurements were performed with an Oxford Instruments System 2000 ac magnetic probe (frequency range 10 Hz–10 kHz, ac RMS field-amplitude up to 5 mT) equipped with a resistive solenoid (maximum dc field 0.13 T) operating in the temperature range $80 < T < 310$ K.

*mehmet.acet@uni-due.de

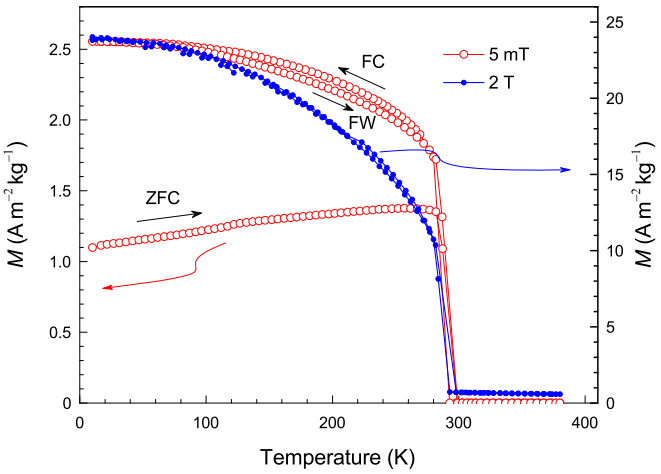

FIG. 1. $M(T)$ obtained under 5 mT and 2 T. The left and right scales are referred to with the arrows. The measurement directions for ZFC, FC, and FW protocols are shown for the 5-mT measurement.

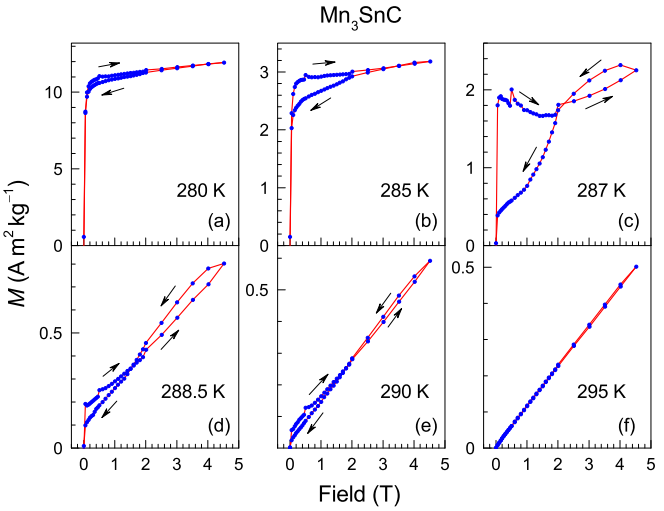

FIG. 2. $M(B)$ in the vicinity of the transition. The arrows indicate the measurement direction. The loops are inverted below about 2 T.

Specific heat measurements under magnetic field were performed with a home-made differential scanning calorimeter (DSC) based on thermoelectric modules [19]. This in-field calorimeter operates under 10^5 mbar vacuum between 250 and 420 K and in magnetic fields up to 1.8 T. Its temperature control resolution is ± 0.01 K and the thermal sweep is controlled by a high-power Peltier cell. The calibration was performed by using a single-crystal sapphire sample. The error of specific heat data is estimated to be about 4%.

The ΔT_{ad} measurements have been performed in a custom designed experimental setup [20]. The measurements were made by turning on and off a low inductive electromagnet, which generates a maximum magnetic field of 1.9 T in a time interval of 1 s. The sample temperature was measured with a Cernox bare-chip resistive temperature sensor having a very small heat capacity.

III. RESULTS

A. Magnetization

Figure 1 shows $M(T)$ for Mn_3SnC measured under a magnetic field of 5 mT and 2 T. With decreasing temperature, a magnetostructural transition takes place at $T_{ms} = 293$ K from a high-temperature PM state to a state with concurrent ferromagnetic/antiferromagnetic (FM/AF) ordering. A weak thermal hysteresis with width of about 2.5 K between the warming and cooling curves is also observed which is related to the first order nature of the transition. $M(T)$ was measured under 5 mT with a zero-field-cooling (ZFC), field-cooling (FC), and field-warming (FW) protocol. The 2-T measurements were made under ZFC and FC conditions; no difference between these two protocols is observed. The 5-mT data on the other hand show a splitting at $T_C = 293$ K related to mixed FM/AF interactions. Other than the hysteresis of the transition, a hysteresis extending from T_{ms} down to low temperatures is also observed. Furthermore, the 5-mT measurement shows a gradual change in $M(T)$ with decreasing temperature below T_{ms} rather than a temperature-independent behavior as would be expected for a FM material reaching the demagnetization limit in small applied fields. These observations are related to the mixed magnetic ordering and interactions and are in agreement previous observations on the irregular magnetic ordering for $T < T_{ms}$ [15].

To examine the properties of the transition in more detail around T_{ms}, we have taken a closer look at the behavior of $M(B)$. The results are presented in Fig. 2 at different temperatures in the field range $0 \leqslant B \leqslant 5$ T. Prior to each measurement, the sample was brought to 305 K and then cooled to the measurement temperature. Data up to 0.5 T are taken in 50-mT intervals, and the interval is increased at higher-field ranges. An unusual behavior between 280–290 K is observed, in which the increasing-field branch up to about 2 T lies at higher values than the decreasing-field branch so that the $M(B)$ loop appears to be inverted in certain field ranges. The effect disappears for $T > T_{ms}$ as seen in the 295-K data and is particularly distinct at 287 K, see Fig. 2(c). Here, the magnetization initially increases rapidly to about 2 A m^2 kg^{-1} and then starts to decrease at 0.2 T showing a spike at 0.5 T. The spike is also observed consistently at this field for all temperatures $T < T_{ms}$. With further increasing field, $M(B)$ still continues to drop up to about 2 T. Above this field, the magnetization rises as the field increases up to 4.5 T. Then, as the field is reduced, $M(B)$ slightly increases and then begins to drop. Below about 2 T, $M(B)$ becomes lower in magnitude than $M(B)$ at corresponding field values on increasing field.

To understand better these anomalous features, we have carried out further detailed $M(B)$ measurements at 287 K. Figure 3 shows $M(B)$ taken for three cycles. The first cycle shows essentially the same behavior and the same anomalies discussed above. Any differences between the data in Fig. 2(c) and the first cycle data in Fig. 3 are related to small differences in the temperature settings. After cycle 1 in Fig. 3, cycle 2 follows a different path running at lower $M(B)$ values. The subsequent cycle 3 shows behavior identical to the second cycle indicating that an equilibrium moment configuration is reached at the end of cycle 1. These data show that there may be time dependencies related to the magnetic ordering process. The characteristic times involved in the ordering

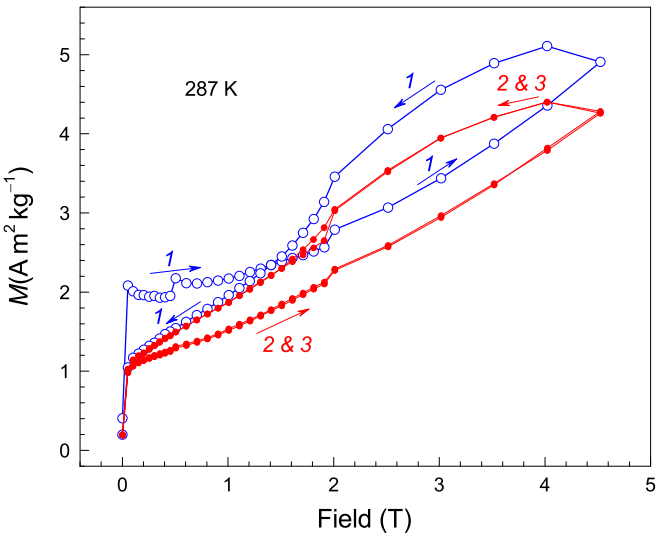

FIG. 3. Consecutively taken $M(B)$ curves. Curve 1 is taken after the sample is cooled in zero-field from 305 to 287 K. This corresponds to the unstable state. The curve is completed after 25 minutes. Curves 2 and 3 are obtained subsequently. They retrace, therefore exhibiting equilibrium state conditions.

process should be the order of times required to complete a magnetization loop in the first cycle, namely, about 35 minutes.

To examine in more detail the magnetization process, we have measured the loop shown in Fig. 4. The field is swept initially in finer steps of 2 mT up to 1.2 T so that the time to complete the loop (red data) is now about 290 min. A second loop is measured directly afterwards (blue data) and is completed in 35 min. The spike feature in the first loop is now more clear, and this loop attains its equilibrium state already at

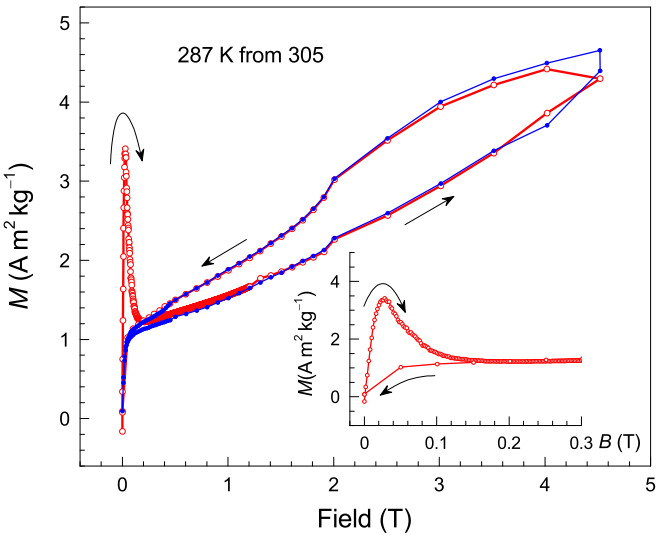

FIG. 4. $M(B)$ taken initially in 2-mT steps. The time to complete a loop is 290 minutes. Arrows indicate the measurement direction. The increasing-field branches of the two curves merge at about 1.4 T. For curve 1, this value is attained in 250 minutes and is the time required for the system to reach equilibrium. The inset shows the low-field-range enlarged.

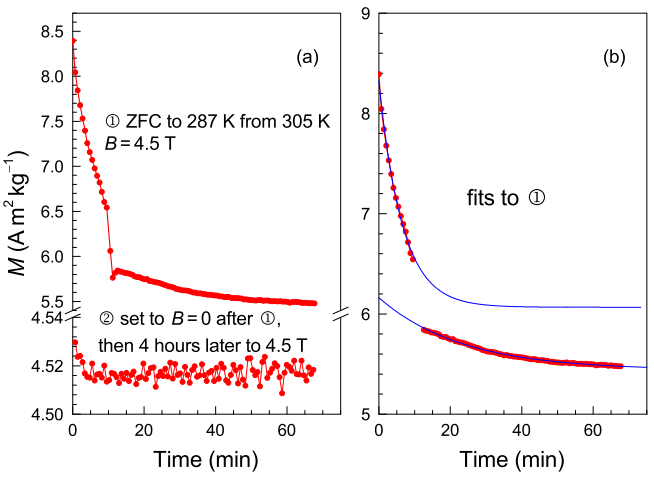

FIG. 5. $M(t)$ measured over 70 min. Curve 1: $M(t)$ starts after firstly cooling the sample in zero-field from 305 to 287 K and subsequently applying a field of 4.5 T. Curve 2: the field is removed and 4 hours later reapplied.

around 1.4 T, which is reached in about 250 min. The low-field details of the initial loop is shown in the inset.

To gain more insight into the nonequilibrium properties of the transition, we have undertaken time-dependent magnetization, $M(t)$, measurements. The results are shown in Fig. 5. The sample is cooled from 305 K in zero field, and a 4.5-T field was applied which itself takes about two minutes to reach. Then, $M(t)$ data were collected over a period of about 70 min. This is shown as the upper curve in Fig. 5(a). This shows initially a fast decrease and then a sudden drop after about 10 min, after which $M(t)$ steadily falls off at a lower rate. Afterwards the field was switched off, and about 4 hours later, the 4.5-T field was reapplied, and again, $M(t)$ was recorded (lower curve). No time dependence is observed in this case.

The data were divided into two parts separated by the discontinuity and an exponential decay function was fitted to each of the data using the relationship

$$M(t) = M_1 \exp^{-t/\tau} + M_\infty, \tag{1}$$

where M_1 is a constant and M_∞ is the value that $M(t)$ approaches at long times. The value of $M(t)$ at $t = 0$ can be calculated from $M(0) = M_1 + M_\infty$. τ is the mean lifetime, for which $\tau = 390$ and 1390 s for the fast and the slow decays, respectively.

B. AC susceptibility

χ_{ac} measurements were carried out in an ac-field of root mean square 0.1 mT and at a frequency of 1 kHz. All data were obtained by bringing the sample to the paramagnetic state by first raising the sample-temperature to 305 K and then cooling it down in zero field to the measurement temperature below the transition. The sample temperature was then allowed to stabilize for about 30 minutes prior to the measurement without applying any magnetic field. The results are shown as a function of applied dc magnetic-field in Fig. 6. Figure 6(a) shows the results of the measurements for all temperatures. The time to complete a measurement, including dc-field

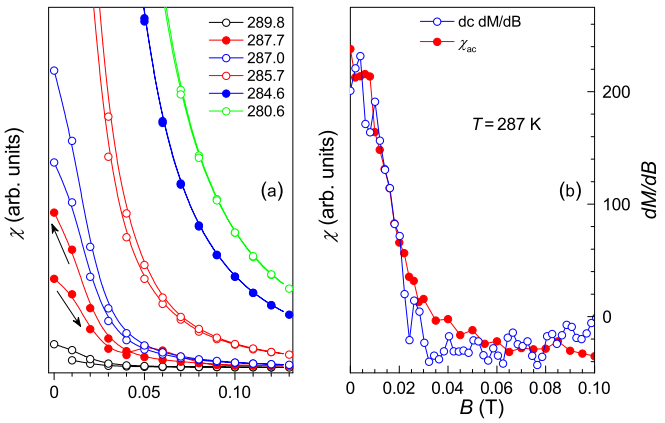

FIG. 6. (a) χ_{ac} measured at 1 kHz and 0.1-mT ac field as a function of applied dc field. (b) comparison of the field derivative of the dc magnetization and χ_{ac} at 287 K.

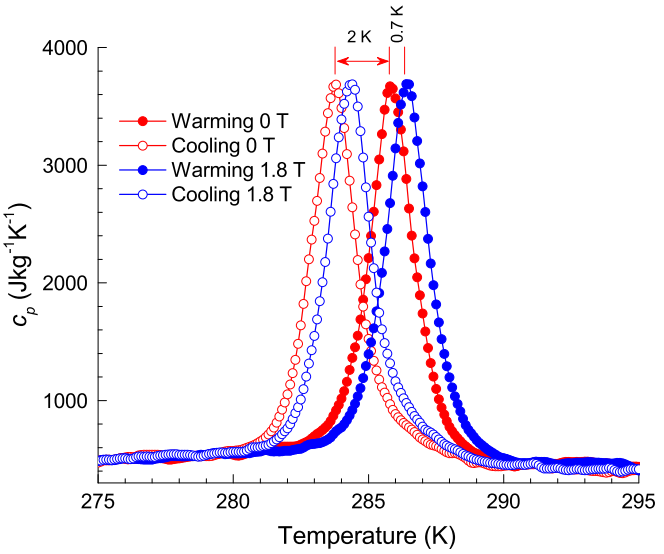

FIG. 7. c_p measured in zero field and in 1.8 T on warming and on cooling. The width of the thermal hysteresis is 2 K. The field-shift of the transition is 0.7 K.

increase and decrease, is about 15 minutes and the dc-field step is 10 mT. The measurement directions are shown with the arrows in the 287.7-K data in Fig. 6(a), and they are similar in the other data, where a difference in the forward and reverse measurement directions is distinctly seen. Initially, on increasing field, χ_{ac}, being the field derivative of the magnetization, is initially large and steadily decreases with increasing field, and eventually the decrease becomes slower. This reflects a small hysteretic behavior with an accompanied remanence. χ_{ac} tends to approach a nonzero steady value at higher fields, which is in accordance with the finite high-field susceptibilities seen in the $M(B)$ data (Fig. 2), being related to the presence of mixed AF/FM coupling.

In order to examine with better detail the isothermal dc-field dependence of ac susceptibility, a measurement was performed at 287 K with a finer dc field step of 2 mT, and the time required to complete the field increasing part turns out to be now 40 minutes. Such measurement was compared in Fig. 6(b) with the field derivative of the dc magnetization corresponding to the field-increasing part of the $M(H)$ curve of Fig. 4. It has to be noted that the time required to reach the field of 100 mT in the $M(H)$ curve of Fig. 4 is of the same order.

C. In-field specific heat and magnetocaloric properties

The DSC measurements were carried out with temperature sweeps on heating and cooling at a rate of 2 K min^{-1}, both in zero magnetic field and in a magnetic field $B = 1.8$ T. The specific heat as a function of temperature, $c_p(T)$, on warming and cooling under zero field and 1.8 T is shown in Fig. 7. A shift of the transition temperature under 1.8 T is about 0.7 K and the width of the thermal hysteresis is 2 K. By integrating the in-field specific heat measurements it is possible to obtain the relative entropy curves of the material as a function of temperature at different magnetic fields. From these, we calculate both the isothermal entropy change and the adiabatic temperature change.

The results for the temperature dependence of the entropy around the transition $S(T)$ and the isothermal entropy change ΔS are given in Fig. 8. Figure 8(a) shows $S(T)$ calculated from $c_p(T)$ spanning the transition region. From these data, ΔS can be determined for both warming and cooling branches as the differences in $S(T)$. The results are shown in Figs. 8(a) and 8(b). The maximum value $\Delta S = 6 \pm 0.4$ J kg^{-1} K^{-1} is in agreement with those obtained for a similar sample from the Maxwell equations [18].

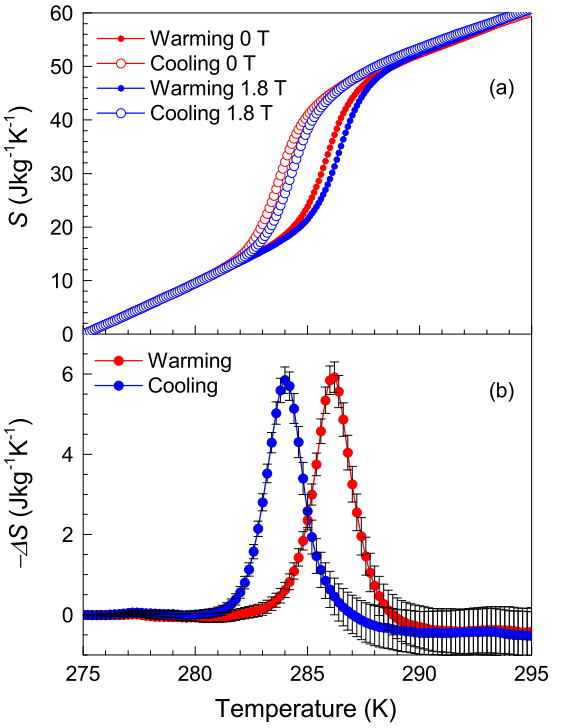

FIG. 8. The entropy at the transition obtained from c_p. (a) $S(T)$ around the transition for the measurement protocols given in the figure. (b) ΔS obtained as the differences of $S(T)$ in zero field and 1.8 T for warming and cooling cases.

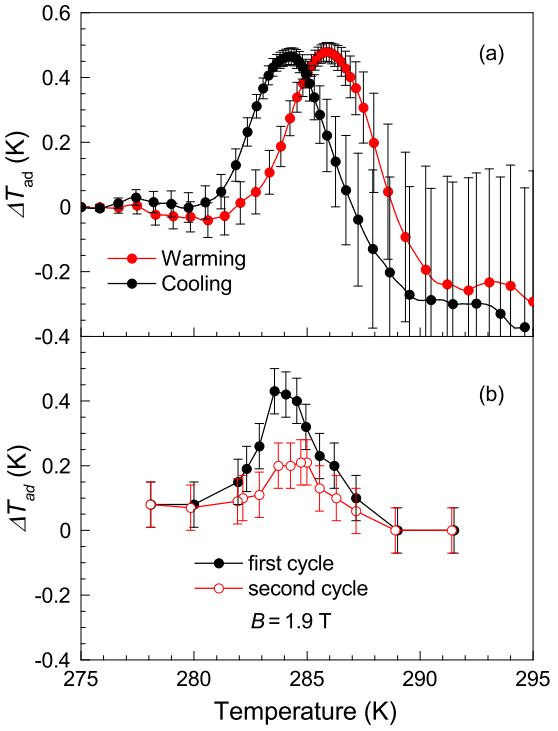

FIG. 9. ΔT_{ad} obtained from (a) c_p and ΔS and (b) from direct adiabatic temperature-change measurements.

$\Delta T(T)$ calculated using $c_p(T)$ is shown in Fig. 9(a). A hysteresis that reflects the hysteresis in c_p is evident with ΔT reaching a maximum value of about 0.5 ± 0.05 K. ΔT was also directly measured by applying a magnetic field change of 1.9 T in 1 s under quasiadiabatic conditions. Direct ΔT measurements are fundamental to probe the material response to the magnetic stimulus under cyclic conditions, because they reflect possible irreversible effects of the transformation (hysteresis, kinetics, structural fatigue), which are not considered in the isofield DSC measurements. The results of direct ΔT measurements are plotted in Fig. 9(b). The direct measurements were carried out for two cycles, namely by applying and removing the field twice. Before each measurement, the sample was warmed up to 305 K in order to reset the high-temperature phase. Figure 9(b) shows, for clarity, only the $\Delta T(T)$ obtained by applying the magnetic field. The first application of the field gives a maximum value for ΔT of about 0.43 ± 0.07 K, which is close to that determined indirectly from c_p. The curves also feature similar forms. On the other hand, the second cycle yields a lower value of about 0.2 ± 0.07 K due to hysteresis losses.

IV. DISCUSSION

A. The magnetization

The results of both $M(H)$ and $M(t)$ measurements show nonergodicity at the magnetostructural transition which is related to the mixed ordering process. If $M(H)$ is measured faster than the characteristic times involved in the ordering process, it shows inverted magnetization loops as in Figs. 3 and 4. The $M(H)$ loops become regular equilibrium loops only after holding the sample just below the transition temperature for several hours or taking the sample to temperatures that are low enough where time-related effects are fast.

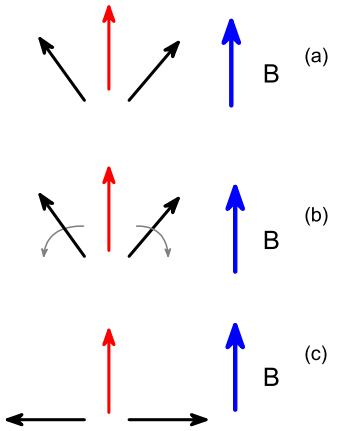

FIG. 10. The sequence of events during the stabilization of the magnetic configuration. (a) The net magnetization is along the field direction. (b) Some moments rotate in a manner as to stabilize AF ordering perpendicular to the direction of FM ordering. (c) The equilibrium configuration.

The inverted hysteresis loops are in fact observable also at lower temperatures, down to 280 K as seen in Fig. 2 so that nonergodic effects may even be present at lower temperatures. In fact, the difference between the FC and FW $M(T)$ curves can be caused by such effects. The FC $M(T)$ curve measured at a sweep rate of 4 K min^{-1} is too fast according to the results shown in Fig. 5 for AF coupling to fully stabilize during the measurement so that FC-$M(T)$ runs at higher values than FW-$M(T)$ curve down to low temperatures.

The spike in $M(H)$ suggests that the mixed FM/AF ordering just below T_{ms} does not occur concurrently but that the AF ordering lags the FM ordering. The initial increase in $M(H)$ at low fields reflects that the system tends to order first ferromagnetically along the 001 direction and only after the field reaches about 30 mT does the AF ordering begin and lead to a rapid decrease in $M(H)$. Depending on the speed at which the field is swept, $M(H)$ can trace a curve which reflects a nonequilibrium or an equilibrium case.

A closer look at the nonergodicity can be taken by observing $M(t)$ along with the depiction in Fig. 10. When the sample is cooled in a field through the transition to a temperature just below T_{ms}, the response of all moments is to align along the field direction as seen in Fig. 10(a). As time progresses, a part of the moments progressively align antiferromagnetically perpendicular to the FM component [Fig. 10(b)] until they reach the equilibrium configuration shown in Fig. 10(c). The initial drop in $M(t)$ in Fig. 5 is rapid and is followed by practically a discontinuity. The initial drop occurs as AF ordering perpendicular to 001 progresses. Since the low-temperature cell volume is larger than the high-temperature volume, mechanical strains during the AF ordering could occur before the equilibrium volume is established so that the discontinuous drop can be initiated when the strain reaches the limit of stabilizing the low-temperature high-volume. After exceeding this threshold, the system continues to relax at a slower rate. The estimated equilibrium value reached by

the fast response $M_{\infty}^{f} = 6.07\,\mathrm{A\,m^2\,kg^{-1}}$ is nearly equal to the estimated value of the initial magnetization of the slow response $M(0) = M_1^s + M_{\infty}^s = 6.15\,\mathrm{A\,m^2\,kg^{-1}}$ verifying that the slow response would take over from the fast response if there were no discontinuity in between. This indicates that the relaxation mechanisms of the stabilization of the AF state are preserved after the discontinuous change. To understand better these mechanisms, time-resolved experiments such as temperature-dependent fast x-ray diffraction is required.

B. Implication on magnetocaloric effects

The complexities encountered in the phase transition in Mn_3SnC is probably not only limited to this material. Other materials known for their favorable magnetocaloric properties could be suffering from mixed AF exchange introduced with time at the transition. The lowering of the overall magnetization due to the rearrangement of the magnetic ordering over time can be causing a lowering of the magnetocaloric effect, which otherwise could be larger if an AF component were not to develop. ΔT_{ad} of Mn_3SnC is only about 0.4 K under 1.8-T field change, however, the virtue of this material is that it exhibits a magnetostructural transition at room temperature, so that if it were to be possible to alleviate AF exchange, the magnetocaloric effect could be enhanced. This could be possible by doping other elements in place of Sn as has been reported in a previous work [18]. The alleviation of AF exchange that could possibly exist in other known materials can be an important task for attaining better magnetocaloric materials.

V. CONCLUSION

We have investigated the time dependence of the magnetic configuration at the mixed magnetic magnetostructural transition in Mn_3SnC and also the specific heat under equilibrium magnetic configurational conditions. Under equilibrium, ΔT obtained indirectly and from direct measurements are in good agreement. The nonergodic nature of the transition involves on the other hand the stabilization of a final configuration that involves additional AF ordering which is not present when the transition is initiated and develops only in time. Elimination of the AF ordering by doping or other external effects such as pressure could enhance the magnetocaloric effect.

ACKNOWLEDGMENT

Work supported by the Deutsche Forschungsgemeinschaft (Germany) (SPP 1599).

[1] T. He, Q. Huang, A. P. Ramirez, Y. Wang, K. A. Regan, N. Rogado, M. A. Hayward, M. K. Haas, J. S. Slusky, K. Inumara, H. W. Zandbergen, N. P. Ong, and R. J. Cava, Nature (London) **411**, 54 (2001).

[2] M. Uehara, T. Yamazaki, T. Kôri, T. Kashida, Y. Kimishima, and I. Hase, J. Phys. Soc. Jpn. **76**, 034714 (2007).

[3] K. Kamishima, T. Goto, H. Nakagawa, N. Miura, M. Ohashi, N. Mori, T. Sasaki, and T. Kanomata, Phys. Rev. B **63**, 024426 (2000).

[4] K. Takenaka and H. Takagi, Appl. Phys. Lett. **87**, 261902 (2005).

[5] K. Takenaka, K. Asano, M. Misawa, and H. Takagi, Appl. Phys. Lett. **92**, 011927 (2008).

[6] T. Tohei, H. Wada, and T. Kanomata, J. Appl. Phys. **94**, 1800 (2003).

[7] M. H. Yu, L. H. Lewis, and A. R. Moodenbaugh, J. Appl. Phys. **93**, 10128 (2003).

[8] Ö. Çakır and M. Acet, Appl. Phys. Lett. **100**, 202404 (2012).

[9] J. P. Bouchaud, R. Fruchart, R. Pauthenet, M. Guillot, H. Bartholin, and F. Chaissé, J. Appl. Phys. **37**, 971 (1966).

[10] D. Fruchart and E. F. Bertaut, J. Phys. Soc. Jpn. **44**, 781 (1978).

[11] Y. B. Li, W. F. Li, W. J. Feng, Y. Q. Zhang, and Z. D. Zhang, Phys. Rev. B **72**, 024411 (2005).

[12] T. Kanomata, T. Kaneko, and Y. Nakagawa, J. Catal. **96**, 451 (1992).

[13] Y. Sun, Y. Guo, Y. Tsujimoto, J. Yang, B. Shen, W. Yi, Y. Matsushita, C. Wang, X. Wang, J. Li, C. I. Sathish, and K. Yamaura, Inorg. Chem. **52**, 800 (2013).

[14] E. T. Dias, K. R. Priolkar, A. K. Nigam, R. Singh, A. Das, and G. Aquilanti, Phys. Rev. B **95**, 144418 (2017).

[15] E. T. Dias, K. R. Priolkar, A. Das, G. Aquilanti, Ö. Çakir, M. Acet, and A. K. Nigam, J. Phys. D **48**, 295001 (2015).

[16] B. S. Wang, P. Tong, Y. P. Sun, X. Luo, X. B. Zhu, G. Li, X. D. Zhu, S. B. Zhang, Z. R. Yang, W. H. Song, and J. M. Dai, Europhys. Lett. **85**, 47004 (2009).

[17] T. Tohei, H. Wada, and T. Kanomata, J. Magn. Magn. Mater. **272**, E585 (2004).

[18] E. T. Dias, K. R. Priolkar, O. Cakir, M. Acet, and A. K. Nigam, J. Appl. Phys. **117**, 123901 (2015).

[19] G. Porcari, F. Cugini, S. Fabbrici, C. Pernechele, F. Albertini, M. Buzzi, M. Mangia, and M. Solzi, Phys. Rev. B **86**, 104432 (2012)

[20] G. Porcari, M. Buzzi, F. Cugini, R. Pellicelli, C. Pernechele, L. Caron, E. Brück, and M. Solzi, Rev. Sci. Instrum. **84**, 073907 (2013).